A Similarity Theory for Unsaturated Downdrafts within Clouds

KERRY A. EMANUEL[1]

Department of Atmospheric Sciences, University of California, Los Angeles 90024

(Manuscript received 18 November 1980, in final form 27 February 1981)

ABSTRACT

Recent observations of cumulus clouds strongly support the hypothesis of Squires (1958) that much of the mixing within such clouds is associated with downward propagating currents initiated near their tops. A similarity theory is here proposed to describe the properties of such currents; the use of similarity is defended on the basis of the observed and predicted scale of the downdrafts. The theory suggests that downward-propagating unsaturated thermals are pervasive throughout all but the largest convective clouds and that quasi-steady unsaturated downdraft plumes may exist in the lower portions of cumulonimbi. In addition to providing a reasonable explanation for the microstructure of and liquid water distribution within cumulus clouds, the theory appears to account for certain severe convective phenomena, including downbursts. A new but related cloud instability is proposed to account for the occurrence of mamma.

1. Introduction

Early aircraft observations of small cumulus clouds (e.g., Malkus, 1954) firmly put to rest any notion that the properties of such clouds could be explained merely by the pseudo-adiabatic ascent of air from cloud base. The observations indicated that the liquid water content and buoyancy of the clouds were far smaller than their respective adiabatic values; indeed, the temperature lapse rate within the clouds closely approximated that of their environment. It was natural to assume, as did Stommel (1947), that as in the case of dry thermals and plumes, most of the discrepancies were due to mixing through the sides of the cloud. Observations (e.g., Warner, 1955) show, however, that little systematic variation in cloud properties occurs across the cloud, in contrast to laboratory plumes and thermals in which the time-mean quantities roughly conform to Gaussian distributions. These and other considerations led Squires (1958) to propose that the bulk of the mixing in such clouds is due to unsaturated downdrafts initiated at the cloud tops and driven by evaporative cooling. Such downdrafts are fundamentally distinct from classical dry or moist convection in that they rely on turbulent mixing to provide simultaneously the liquid water and dry air necessary for evaporative cooling. The phenomenon is therefore peculiar to clouds. Squires (1958) was able to show, using a simple model employing constant eddy mixing, that such downdrafts are capable of penetrating to great depths within typical clouds.

Squires' idea is particularly attractive as it accounts for many of those observed properties of cumulus clouds which cannot be explained by simple entraining plume models. These characteristics include the lateral distribution of cloud properties, the magnitude of the ratio of actual to adiabatic liquid water content (Warner, 1970), the frequent appearance of dry holes in the bases of clouds (Warner, 1955), the weak dependence of maximum liquid water content on cloud diameter in all but the smallest clouds (Squires, 1958), and the breakup of cloud updraft at higher levels (Malkus, 1954). In light of these observations and Squires' theory, it seems surprising that many theoretical investigations of cumulus dynamics continue to rely on lateral entrainment to provide the necessary mixing. This weakness is especially apparent in cumulus parameterization schemes.

A recent aircraft study of Colorado cumulus clouds by Paluch (1979) shows rather dramatically that the properties of air deep within the clouds are attributable primarily to the mixing of air from below cloud base with environmental air from near the cloud top, rather than by mixing with environmental air originating near or below the level where the measurements were taken. In her investigation, Paluch identifies two adiabatically invariant scalar quantities which mix in a linear or nearly linear fashion. These quantities are the total water content Q (when precipitation-size particles are absent) and a modified equivalent potential temperature θ_q. These are measured by aircraft within the clouds and plotted together with an environmental sounding of the same quantities in a Q-θ_q coordinate system. The measurements

[1] Present affiliation: Department of Meteorology and Physical Oceanography, MIT, Cambridge, MA 02139.

0022-4928/81/081541-17$08.25

generally fall along a straight line connecting points on the environmental curve representing sub-cloud and cloud-top air, respectively, suggesting that the mixture involves relatively little environmental air from middle levels. This is perhaps the first persuasive study of the origin of air within extratropical cumulus clouds.

In a review of turbulence and mixing processes in cloud dynamics, Telford (1975) suggests that penetrative downdrafts are the dominant mixing process in clouds and points out that the scale of the former is such that they are not resolvable in most numerical cloud models; neither can most turbulence parameterizations adequately account for their existence. Telford proposes that small cumuli are nearly in hydrostatic equilibrium with their environment, the equilibrium being brought about by the cooling effect of penetrative downdrafts. His calculation of the liquid water content of equilibrium clouds is in good agreement with observations.

Subsequent to Squires' (1958) initial analysis, little has been done in the way of describing the individual unsaturated downdrafts. In the following section, the capacity of similarity theory to adequately describe the dynamics of unsaturated downdrafts is explored.

2. On the use of similarity theory in describing penetrative unsaturated downdrafts

The description of the mean properties of fully turbulent dry convective plumes and thermals using similarity theory has been developed primarily by Schmidt (1941), Batchelor (1954) and Morton *et al.* (1956). The latter group also were among the first to carry out detailed measurements of laboratory plumes and thermals in stratified fluids. The similarity theory is found to provide an excellent description of the laboratory phenomena.

The basic assumptions on which the similarity theories rely are that (i) the radial profiles of vertical velocity and buoyancy are geometrically similar at all heights, (ii) the mean rate of entrainment of environmental fluid is proportional at all heights to a characteristic mean velocity, and (iii) local variations of density throughout the convective elements are small compared to a reference density. It is further assumed that the environment of the convective elements is stationary, and that the convective elements are steady in some coordinate system. The stationary environment is applicable to convection which is fundamentally local rather than global in character; in the latter case the entire fluid is presumed to be in motion, rendering useless the concept of maintained or instantaneous point sources.

The fundamental premise upon which assumptions (i) and (ii) strongly rely is that no velocity or length scales may be formed from the parameters specifying the boundary and initial conditions of the fluid system. In that case, the length scales describing the size of turbulent eddies and the lateral variation of mean velocity and buoyancy may only depend on the distance at any time from the source. This will be precisely the case, for example, in a plume over a maintained point source of heat in a semi-infinite homogeneous fluid, provided that the Reynolds number is effectively infinite and that the buoyancy is small compared to the acceleration of gravity. Then the only relevant boundary condition is the maintained buoyancy flux, from which one cannot form a length scale. If the fluid is stably stratified, however, an external length scale can be formed from the boundary buoyancy flux and the Brünt-Väisälä frequency; this scale determines the maximum penetration height of the plume and makes questionable the similarity assumption. Morton *et al.* (1956) have shown that in this case, the similarity description fails only near the top of the plume and still provides a useful description of the plume properties in its middle and lower sections.

The similarity approach, however, cannot be adequate for treating the dynamics of cumulus clouds since these merely represent the ascending branches of a global instability and, as such, must possess horizontal scales which are related to the vertical scale of the unstable layer. Indeed, the visual appearance of cumulus clouds strongly suggests a fundamental relationship between vertical and horizontal scales and does not suggest the conical expansion of plumes over a point source of heat. It must be pointed out, however, that moist convective updrafts are more local in character than their dry counterparts since the one-way nature of the condensation insures that the dry environmental downdrafts will be relatively weak and broad compared to the cloudy updrafts.

The dynamics of evaporatively driven penetrative downdrafts are fundamentally distinct from those of moist convective updrafts in that mixing is *necessary* to sustain the former, while it always works against the latter. Thus cumulus clouds are relatively broad so as to minimize the effects of lateral entrainment, while the scale of penetrative downdrafts is small enough that lateral entrainment can provide the liquid water necessary to drive the downdraft. Observations of cumulus clouds (Warner, 1955; McCarthy, 1974) suggest that lateral entrainment is important only in clouds with diameters $\lesssim 1$ km, while the scale of the horizontal fluctuations of vertical velocity, liquid water content and buoyancy within larger clouds is very much smaller than the lateral dimensions of the clouds themselves (e.g., Malkus, 1954; Warner, 1955; Warner and Squires, 1958). As in the case of moist convection, the one-way nature of the penetrative downdraft process insures that downdrafts resulting purely from the cloud-top instability will be relatively intense and isolated, while any

upward return circulation forced by the downdrafts will be broad and weak. Deardorff (1980) suggests that this is the case for penetrative downdrafts in stratocumuli. The isolated character of penetrative downdrafts may not apply near the tops of growing cumuli, where the downdrafts are probably initiated by the static instability in the upper portion of the cloud.

These ideas suggest that in the ideal case of an inert, homogeneous cloud of great vertical extent, the lateral scale of penetrative downdrafts is internally rather than externally determined and, to the extent to which this is true, their dynamics may be described using the similarity approach. While it must be admitted that clouds, especially cumulus clouds, are far from being homogeneous and inert, it appears that the similarity approach may constitute a plausible means of isolating and highlighting the dynamics of the individual penetrative downdrafts. The theory, which ideally pertains to the properties of unsaturated plumes and thermals in deep, inert clouds, provides a wealth of physical insight regarding the dynamics of these motions. We therefore proceed by developing one-dimensional equations describing the radially averaged properties of evaporatively cooled unsaturated plumes and thermals.

3. Penetrative plumes

Penetrative convection can occur when the environmental air overlying the cloud is sufficiently cool and dry. When such air is mixed downward into the cloudy air, the cloud water evaporates and cools the mixture to the point where it is negatively buoyant with respect to the surrounding cloudy air; hence it accelerates downward. Were it not for the effect of water vapor and liquid water on the buoyancy of air, it could be easily seen that the criterion for this instability is that the moist static energy h of the overlying environmental air be less than that of the cloudy air. In fact, the effect of liquid water and water vapor is not negligible, as shown by Randall (1980) who states the exact instability criterion

$$\Lambda h < \alpha L_v \Delta(q + l),$$

where

$$\alpha \equiv \frac{c_p T}{L_v}\left[\frac{1 + \frac{L_v}{c_p}\left(\frac{\partial q^*}{\partial T}\right)_p}{1 + (1+\gamma)T\left(\frac{\partial q^*}{\partial T}\right)_p}\right],$$

$$\nu = 0.608$$

and q^* is the saturation mixing ratio. Δh and $\Delta(q + l)$ are the jumps across cloud top of moist static energy and total water, respectively. Since the latter is generally negative, the actual criterion for instability is more stringent than $\Delta h < 0$.

Depending on the degree of instability, the initiation of the downward convection may be characterized by the magnitude of the downward fluxes of negative buoyancy and total water deficit which result from the instability. We shall use these fluxes as initial or boundary conditions for penetrative convection under the assumption that the cloud-top instability criterion is satisfied.

The derivation of conservation equations describing the radially averaged properties of a cylindrically symmetric steady plume descending from a maintained point source closely follows the development of the plume equations given by Morton *et al.* (1956). The assumptions regarding the nature of the plume are as follows:

(i) Radial profiles of vertical velocity, buoyancy and water vapor are geometrically similar at all heights.

(ii) The mean entrainment velocity is proportional to the radially averaged vertical velocity.

(iii) The total buoyancy is small compared to the acceleration of gravity.

(iv) The Froude number is small.

(v) Molecular viscosity is negligible, i.e., the plume is fully turbulent.

(vi) The environment is stationary or moving with uniform vertical velocity.

Assumptions (i), (ii), (iii) and (vi) have been discussed in Section 2. The assumption that the Froude number is small asserts that, as a result of the small scale of the plume, aerodynamic effects are negligible compared to buoyant accelerations; this assumption together with (v) have been very well supported by laboratory experiments.

An additional assumption also must be made with regard to the effects of phase transition:

(vii) All entrained liquid water evaporates immediately provided the plume is unsaturated.

This assumption will be very nearly valid for liquid cloud droplets, but must fail for precipitation particles. The evaporation of entrained ice will be discussed in Section 6.

On the basis of laboratory measurements, Morton *et al.* (1956) assume a Gaussian radial distribution of the scalar plume quantities. This assumption poses a special problem in the present case since the liquid water deficit cannot have a Gaussian distribution unless the plume is unsaturated only at its central axis. We therefore assume top-hat profiles for the plume quantities in the present case, recognizing that the shape of the assumed profile only affects certain numerical constants and does not alter the sought-for parameter dependences.

The plume is taken to propagate downward from $z = 0$ so that the entrainment assumption takes the

form

$$\bar{u} = \alpha w,$$

where $\bar{u}$ is a mean radial turbulent entrainment velocity, w the plume vertical velocity (taken to be negative), and α the entrainment constant.

Following Morton *et al.* (1956), the radially integrated conservation equations for mass (excluding water vapor) and momentum are

$$\frac{d}{dz}(R^2w) = -2R\alpha w, \tag{1}$$

$$\frac{d}{dz}(R^2w^2) = R^2(B + gl_c), \tag{2}$$

where $R(z)$ is the plume radius and $B(z)$ is the plume temperature surplus, defined as

$$B \equiv g\left(\frac{T_{vp} - T_{vc}}{\bar{T}_v}\right),$$

where T_{vp} and T_{vc} are the virtual temperatures of the plume and cloud, respectively, $\bar{T}_v$ is a constant reference virtual temperature, and g is the acceleration of gravity. The momentum equation (2) includes the hydrostatic effect of the cloud liquid water mixing ratio l_c on the density deficit of the plume. The total plume buoyancy is then $B + gl_c$.

The conservation equations for heat and water may be derived by first considering the radially integrated conservation equation for any quantity A conserved in moist-adiabatic processes. The steady-state, Boussinesq conservation equation for A may be written

$$\nabla\cdot\mathbf{V}A = 0.$$

Integrating the above over a slice of the plume of depth Δz and radius R and applying the divergence theorem yields

$$2\pi R\Delta z\alpha wA_c + \pi(R^2wA_p)_{z+\Delta z} - \pi(R^2wA_p)_z = 0,$$

where A_p and A_c are the scalar quantity in the plume and surrounding cloud respectively. Dividing through by Δz and taking the limit as $\Delta z \to 0$, the above becomes

$$-2R\alpha wA_c = \frac{d}{dz}(R^2wA_p).$$

Using (1) we can write the above as

$$A_c\frac{d}{dz}(R^2w) = \frac{d}{dz}(R^2wA_p)$$

or alternatively

$$\frac{d}{dz}[R^2w(A_p - A_c)] = -R^2w\frac{dA_c}{dz}. \tag{3}$$

One quantity which is nearly conserved in a reversible moist-adiabatic process is the liquid water static energy defined as

$$h_l \equiv c_{pv}T + gz - L_vl,$$

where c_{pv} is a weighted average heat capacity for moist air. The replacement of c_{pv} by its dry equivalent c_p introduces a small error; however, it can be shown that the quantity c_pT_v is a closer approximation to $c_{pv}T$ than is c_pT. Thus we define a virtual liquid water static energy

$$h_{lv} \equiv c_pT_v + gz - L_vl$$

and take this to be nearly conserved in a moist adiabatic process. Multiplying h_{lv} through by $g/c_p\bar{T}_v$ and substituting into (3) yields

$$\frac{d}{dz}[R^2w(B + Ml_c)] = -R^2w\frac{d}{dz}\left(\frac{g}{c_p\bar{T}_v}h_{lvc}\right), \tag{4}$$

where M is a latent heat constant defined as

$$M \equiv \frac{L_vg}{c_p\bar{T}_v}.$$

The right-hand side of (4) also may be written

$$-R^2w\left(N^2 - M\frac{dl_c}{dz}\right),$$

where

$$N^2 \equiv \frac{g}{\bar{T}_v}\left(\frac{dT_{vc}}{dz} - \Gamma\right).$$

Here N is a Brünt-Väisälä frequency and Γ the dry adiabatic lapse rate.

A further conservative property in a strictly reversible moist-adiabatic process is the total water L, where

$$L = q + l$$

and q is the vapor mixing ratio. Substituting the above into (3) and assuming that the plume is unsaturated and contains no liquid water, we obtain

$$\frac{d}{dz}[R^2w(q - L_c)] = -R^2w\frac{dL_c}{dz}, \tag{5}$$

where L_c is the total water of the surrounding cloud.

The set (1), (2), (4) and (5) can be somewhat simplified by introducing new dependent variables proportional to the mass, momentum, buoyancy and water deficit fluxes. These are

$$X \equiv R^2w,$$

$$U \equiv Rw,$$

$$F \equiv R^2wB,$$

$$Q \equiv R^2w(q - L_c).$$

In terms of these new variables, we may conveniently specify boundary conditions at $z = 0$. Fol-

lowing Morton *et al.* (1956), the mass and momentum fluxes are taken to be zero while finite buoyancy and water deficit fluxes are specified at $z = 0$. This specification will lead to infinite buoyancy and water deficit at $z = 0$, which artificiality is attributable to the use of a point source. The physical consequences of this artificiality can be circumvented to a degree, for any physical problem, by defining a "virtual source" where the projection of the observed plume boundaries intersect at $z > 0$. The boundary conditions may be written

$$\left.\begin{aligned} X &= U = 0 \\ F &= F_0 \\ Q &= Q_0 \end{aligned}\right\} \quad \text{at} \quad z = 0.$$

For the sake of simplicity, we will examine the case of a cloud in which the static stability, liquid water and lapse rate of mixing ratio are all constant. (The lapse rate of mixing ratio only affects the water deficit budget and does not affect the dynamics of the plume except in so far as it determines whether or not the plume becomes saturated.) For these simple cloud conditions, the conservation equations can be considerably simplified by introducing nondimensional dependent and independent variables. Denoting the old dimensional variables by asterisks, the new variables are defined

$$X^* \equiv 2^{5/8}\alpha^{1/2}N^{-5/4}F_0^{3/4}X,$$

$$z^* \equiv 2^{-5/8}\alpha^{-1/2}N^{-3/4}F_0^{1/4}z,$$

$$U^* \equiv 2^{1/4}N^{-1/2}F_0^{1/2}U,$$

$$l_c^* \equiv 2^{-5/8}\alpha^{-1/2}N^{5/4}F_0^{1/4}M^{-1}l_c,$$

$$F^* \equiv F_0F,$$

$$Q^* \equiv F_0N^{-2}\left(-\frac{dq_c^*}{dz^*}\right)Q.$$

Using these new variables, the dimensionless forms of (1), (2), (4) and (5) are

$$\frac{dX}{dz} = -U \qquad \text{mass,} \qquad (6)$$

$$\frac{dU^4}{dz} = X(F + gM^{-1}Xl_c) \qquad \text{momentum,} \qquad (7)$$

$$\frac{dF}{dz} = -X - \frac{d}{dz}(Xl_c) \qquad \text{heat,} \qquad (8)$$

$$\frac{dQ}{dz} = X \qquad \text{water,} \qquad (9)$$

and the boundary conditions are

$$\left.\begin{aligned} X &= U = 0 \\ F &= 1 \\ Q &= Q_0{}^*F_0{}^{-1}N^2\left(-\frac{dq_c^*}{dz^*}\right)^{-1} \end{aligned}\right\} \quad \text{at} \quad z = 0. \qquad (10)$$

The set (6)–(8) is identical to that derived by Morton *et al.* (1956) except for the additional terms in the momentum and heat equations describing, respectively, the effects of cloud water on plume buoyancy and the evaporation of liquid water. Note that (9) is independent of (6)–(8) except that a prediction of saturation invalidates the assumptions underlying (7) and (8). Also note that (7) is the only nonlinear equation.

Eqs. (6)–(8) are numerically integrated using simple forward differencing and a dimensionless increment in z of -0.01. The integration is started by solving analytically the difference equations associated with (6)–(8) to approximately first order in Δz. This results in

$$U(\Delta z) = -4^{-1/3}(-\Delta z)^{2/3},$$

$$X(\Delta z) = -2^{-5/3}(-\Delta z)^{5/3},$$

$$F(\Delta z) = 1 + 2^{-5/3}(-\Delta z)^{5/3}l_c.$$

The integration is carried forward until U vanishes.

The water deficit equation (9) has an analytic solution in terms of the buoyancy flux F, the mass flux X and the cloud liquid water. By eliminating X between (8) and (9) there results

$$\frac{d}{dz}(F + Q + Xl_c) = 0.$$

This integrates to

$$F + Q + Xl_c = 1 + Q_0, \qquad (11)$$

where Q_0 is the normalized initial water deficit flux. The actual saturation deficit of the plume can be deduced using the Clausius-Clapeyron equation to relate the mixing ratio of the plume to that of its cloudy environment; the latter is assumed saturated. Thus the average saturation mixing ratio within the plume may be expressed approximately as

$$q_s^* \approx q_c^* \exp\left(\frac{L_v}{R_v\bar{T}g}B^*\right), \qquad (12)$$

where q_s^* and q_c^* are the saturation mixing ratios of the plume and cloud, L_v and R_v are the latent heat of vaporization and the gas constant for water vapor, $\bar{T}$ is a mean reference temperature, and B^* is the dimensional plume heat surplus. Dividing (11) through by X and subtracting the normalized form

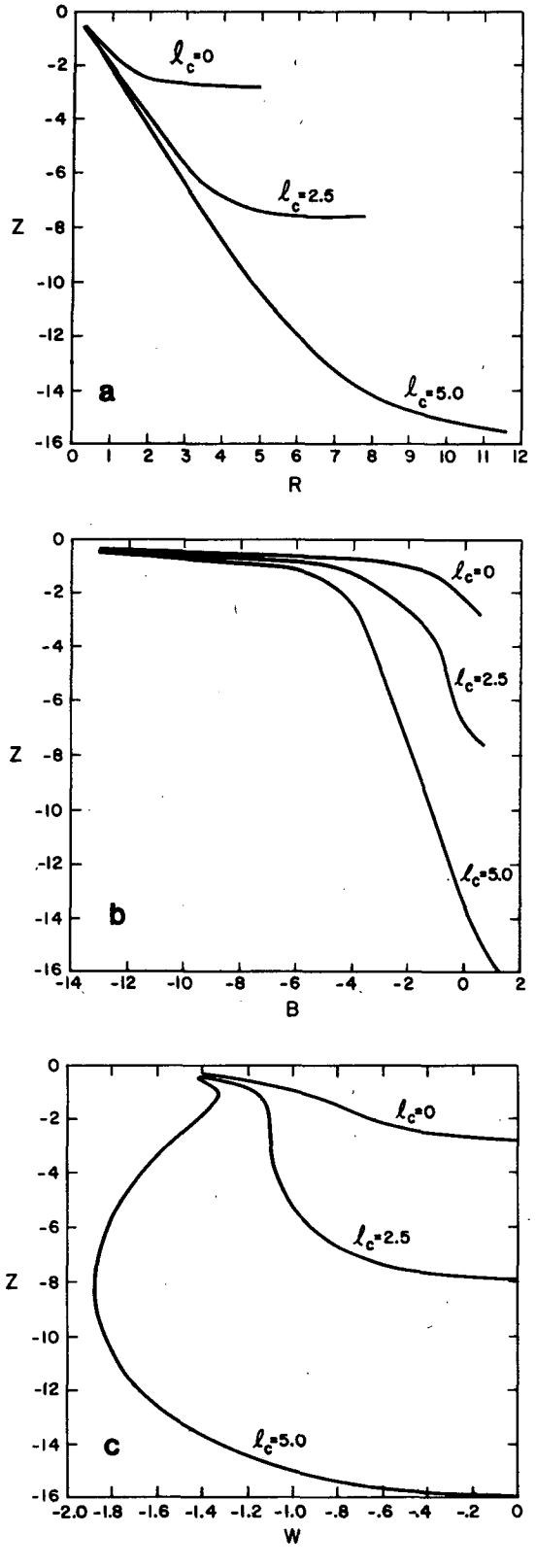

FIG. 1. Nondimensional plume radius R, buoyancy B and vertical velocity W as functions of dimensionless depth, for three values of the normalized cloud water content (l_c).

of (12), one obtains

$$q_s - q = q_c(e^{aB} - 1) + B + \left[1 - \frac{N^2}{M}\left(-\frac{dq_c^*}{dz^*}\right)^{-1}\right] l_c - \frac{1 + Q_0}{X}, \quad (13)$$

where the mixing ratios have been normalized via

$$q^* = 2^{-5/8}\left(-\frac{dq_c}{dz}\right) F_0^{1/4} N^{-3/4} \alpha^{-1/2} q$$

and a is defined

$$a \equiv L_v R_v^{-1} \bar{T}^{-1} g^{-1} 2^{-5/8} N^{5/4} F_0^{1/4} \alpha^{-1/2}.$$

By inspection of (13), one observes that since B is generally negative, a necessary but insufficient condition for the plume to remain unsaturated at large X is that

$$\left(-\frac{dq_c^*}{dz^*}\right) > \frac{N^2}{M}, \quad (14)$$

which is equivalent to the requirement that the moist static energy decrease upward in the cloud. This is likely to be the case in most clouds except those which contain moist-adiabatic updrafts. Exact profiles of the saturation deficit may be constructed using (13) once the dimensionless buoyancy and mass flux are determined.

The solutions for the steady plume radius, buoyancy and vertical velocity as functions of z are shown in Fig. 1 for three values of the normalized cloud water content l_c. The computations have been carried out under the assumption that the plume remains unsaturated. The solution for $l_c = 0$ is identical to that obtained by Morton *et al.* (1956) and has been presented for comparison. The quantities plotted have been normalized according to

$$\left.\begin{aligned} R^* &= 2^{3/8}\alpha^{1/2}N^{-3/4}F_0^{1/4}R \\ B^* &= 2^{-5/8}\alpha^{-1/2}N^{5/4}F_0^{1/4}B \\ W^* &= 2^{-1/8}\alpha^{-1/2}N^{1/4}F_0^{1/4}W \end{aligned}\right\}.$$

The plumes trace out nearly conical cross sections until they are within ~20% of their maximum penetration depths; moreover, the vertex angle of the cone is a very weak function of the cloud liquid water content. The magnitude of the heat deficit is always a monotonically decreasing function of depth while the depth at which the temperature deficit of the plume vanishes is very close to the bottom of the plume. (The total buoyancy, which includes the effect of liquid water on cloud density, vanishes at a somewhat higher level within the plume.) The magnitude of the vertical velocity is also a monotonic function of depth for normalized liquid water content $\lesssim 2.5$; for greater values of cloud water the vertical velocity has a maximum negative value at a depth of roughly half the total vertical extent of the plume.

Simple curve fits describing the maximum dimensionless penetration depth and vertical velocity of the plume as a function of cloud liquid water yield

$$\left.\begin{aligned} -z_{max} &= 2.83 + 1.38 l_c^{7/5} \\ -w_{max} &= 0.17 + 0.34 l_c \end{aligned}\right\}, \quad l_c \geq 2.5.$$

In dimensional form, these expressions are

$$\left.\begin{aligned} -z^*_{max} &= 1.835 F_0^{1/4} N^{-3/4} \alpha^{-1/2} \\ &\quad + 1.620 \alpha^{1/5} N^{-5/2} F_0^{-1/10} M^{7/5} l_c^{*7/5} \\ -w_{max} &= 0.156 F_0^{1/4} N^{1/4} \alpha^{-1/2} \\ &\quad + 0.481 N^{-1} M l_c^* \end{aligned}\right\}, \quad l_c \geq 2.5.$$

Note that the terms containing the dependence on liquid water have relatively weak dependences on the initial buoyancy flux and the entrainment parameter α. Table 1 shows maximum plume penetrative depths and vertical velocity as functions of cloud water content for typical values of cloud static stability and initial buoyancy flux. The value of α is taken to be 0.20 to be consistent with the measurements of dry laboratory plumes by Morton *et al.* (1956); the penetration depths are computed assuming that saturation does not occur.

One observes that the plumes are capable of descending through rather large depths if they remain unsaturated, which condition, according to (13), may be realized if the moist static energy decreases upward sufficiently rapidly. The penetration depths are probably somewhat overestimated due to the use of a top-hat profile.

As mentioned previously, the penetration depth of the plume is limited, if not by saturation, by the monotonic downward decrease of its surface area-to-volume ratio to the extent that insufficient cloud water is entrained and evaporated to sustain the negative buoyancy against adiabatic warming. In an actual penetrative plume, however, the buoyancy should first become positive near the central axis if the air contains no liquid water there. This may lead to reversed vorticity generation near the central axis and the eventual splitting of the plume into several smaller elements. The possibility, therefore, of a branching behavior should be considered. We will return to this question in the following section.

TABLE 1. Maximum penetration depth and vertical velocity (where applicable) of penetrative plumes as a function of cloud liquid water content. Calculations are performed assuming the plume remains unsaturated, and for $N^2 = 5 \times 10^{-5}$ s^{-2}, $\alpha = 0.20$, $M = 82$ m^2 s^{-1} and $F_0 = 350$ m^4 s^{-3}. The maximum penetration depth is insensitive to the value of F_0 except when $l_c = 0$.

l_c (g kg^{-1})	$-z_{max}$ (km)	$-w_{max}$ (m s^{-1})
0	0.73	—
0.5	2.50	—
1	5.42	6.02
2	13.10	11.59
3	22.55	17.17
4	33.38	22.75
5	45.35	28.33

4. Penetrative thermals

Idealized laboratory convection is generally produced by maintained localized sources of buoyancy or the instantaneous release of a small volume of buoyant fluid within a much larger volume of stationary fluid. In the former case a steady plume is produced while in the latter a discrete element is generated. While the arguments presented in Section 2 suggest that similarity theory ought to describe well the properties of penetrative downdrafts, there is little to suggest whether the downdrafts take the form of steady plumes or thermals, or perhaps a quasi-periodic succession of thermals which behave in some ways like both of these forms of convection. In any event, the general properties of penetrative downdrafts ought to be illuminated by examining the characteristics of both pure plumes and thermals.

The derivations of Morton *et al.* (1956) are again closely followed in the present treatment of discrete penetrative thermals. The same basic assumptions are made regarding the radial distribution of thermal properties, the self-similarity and the entrainment. The latter is in this case characterized by a mean inflow velocity over the entire surface of the thermal, which is assumed to be spherical (the assumption regarding the thermal's geometry again only affects the numerical constants). The conservation equations for the total time rate of change of mass, momentum, heat and water deficit are

$$\frac{d}{dt} R^3 = -3R^2 \alpha w \qquad \text{mass,} \qquad (15)$$

$$\frac{d}{dt} R^3 w = R^3 (B + g l_c) \qquad \text{momentum,} \qquad (16)$$

$$\frac{d}{dt} R^3 B = -N^2 R^3 w - M l_c \frac{d}{dt} R^3 \qquad \text{heat,} \qquad (17)$$

$$\frac{d}{dt} R^3 (q - L_c) = -R^3 \frac{d}{dt} L_c \qquad \text{water deficit,} \qquad (18)$$

where R is the mean thermal radius and the remaining variables are defined as before. For convenience, the independent variable may be transformed from time to height using

$$\frac{d}{dt} = \frac{dz}{dz} \frac{d}{dz} = w \frac{d}{dz}.$$

For convenience in defining the boundary conditions, new dependent variables proportional to volume, kinetic energy, total water deficit and total

heat deficit are defined as follows:

$$\left.\begin{aligned} V &\equiv R^3 \\ K &\equiv w^2 \\ Q &\equiv R^3(q - L_c) \\ F &\equiv R^3 B \end{aligned}\right\}. \tag{19}$$

In terms of the new variables, the conservation equations (15)–(18) are written

$$\frac{dV}{dz} = -3\alpha V^{2/3}, \tag{20}$$

$$\frac{dK}{dz} - 6\alpha K V^{-1/3} = 2FV^{-1} + 2gl_c, \tag{21}$$

$$\frac{dF}{dz} = -N^2 V - Ml_c \frac{dV}{dz}, \tag{22}$$

$$\frac{dQ}{dz} = -V \frac{dL_c}{dz}. \tag{23}$$

The boundary conditions defining a point source of heat and water deficit at $z = 0$ are

$$\left.\begin{aligned} V &= K = 0 \\ F &= F_0 \\ Q &= Q_0 \end{aligned}\right\}, \quad \text{at} \quad z = 0. \tag{24}$$

For simplicity, we again treat the case of constant N, constant cloud water l_c and constant lapse rate of cloud saturation mixing ratio. As in the case of dry thermals, the penetrative thermal equations have analytic solutions which can be arrived at by solving (20), (22) and (21) in that order. The water deficit equation (23) can also be solved given the solution of (20). For clarity, we express the solutions in terms of the radius, vertical velocity, heat and saturation deficit:

$$R = -\alpha z, \tag{25}$$

$$w^2 = -\tfrac{1}{2}\alpha^{-3}F_0 z^{-2} - \tfrac{2}{7}(M - g)l_c z - \tfrac{1}{16}N^2 z^2, \tag{26}$$

$$B = -F_0\alpha^{-3}z^{-3} - Ml_c - \tfrac{1}{4}N^2 z, \tag{27}$$

$$(q_s - q) = Q_0\alpha^{-3}z^{-3} - l_c + q_c\left[\exp\left(\frac{L_v}{R_v\bar{T}g}B\right) - 1\right] - \frac{1}{4}\left(-\frac{dq_c}{dz}\right)z. \tag{28}$$

The last expression has been derived from (23) and the Clausius-Clapeyron equation (12); the subscripts zero denote the initial values of the quantities. The expression (28) clearly shows the various contributions to the moisture budget. The first term on the right is the contribution from the initial flux of water deficit and decays as z^{-3}, while the second term results from the entrained cloud liquid water. The third term represents the effect of the thermal's temperature deficit on the saturation mixing ratio, and the last term represents the effect of the increasing cloud mixing ratio along the path of the thermal. The depth at which saturation will occur, provided the vertical velocity is still negative and finite, can be obtained from (28). The third term on the right of (28) can usually be neglected in this calculation provided that saturation does not occur too close to the initial source. Provided that

$$l_c \gg 2^{-3/2}\alpha^{-3/4}(-Q_0)^{1/4}\left(-\frac{dq_c}{dz}\right)^{3/4},$$

analysis of the balance of the remaining terms reveals that the level at which saturation occurs is approximately

$$-z_{\text{sat}} \approx \alpha^{-1}(-Q_0)^{1/3}l_c^{-1/3}. \tag{29}$$

A more precise analysis of (28) shows that saturation will never occur if

$$-Q_0 \geq 6.75 l_c^4\alpha^3\left(-\frac{dq_c}{dz}\right)^{-3}. \tag{30}$$

These conditions on the initial flux of water deficit are ultimately related to the cloud-top instability criterion.

Provided that the thermal remains unsaturated, the maximum penetration depth and maximum vertical velocity attained by the descending thermal may be assessed using (26). Analysis of the dominant balance of terms in (26) shows that the first term on the right may be neglected in computing the maximum penetration depth and vertical velocity if

$$l_c \gg F_0^{1/4}\alpha^{-3/4}N^{3/2}(M - g)^{-1}.$$

The right-hand side of the above is $O(10^{-5})$ so that the condition is easily satisfied even in small clouds. Neglecting the first term on the right of (26), then, the maximum penetration depth is

$$-z_{\max} = \tfrac{32}{7}(M - g)N^{-2}l_c \tag{31}$$

and the maximum vertical velocity is

$$-w_{\max} = \tfrac{4}{7}(M - g)N^{-1}l_c, \tag{32}$$

occurring at a height

$$-z = \tfrac{16}{7}(M - g)N^{-2}l_c. \tag{33}$$

Note that the maximum vertical velocity occurs at exactly half the maximum penetration depth and that none of the above expressions depends on the initial conditions or the entrainment parameter. The maximum penetration depth and vertical velocity depend linearly on the liquid water concentration. Table 2 shows these quantities as a function of liquid water concentration for comparison with the plume quanti-

ties listed in Table 1. It is assumed that the thermal remains unsaturated.

It is again evident that penetrative convection can reach great depths at characteristic velocities similar to those associated with typical convective updrafts. As in the case of the plume, the thermal loses its negative buoyancy when the surface-area-to-volume ratio becomes too small for the entrainment and evaporation of liquid water to keep pace with adiabatic warming.

In the case of laboratory dry thermals, the motion follows a damped oscillation after the maximum height has been attained. In the present example, however, a different behavior is implied. Unlike the dry thermal, the penetrative thermal, were it to come to rest at its maximum penetration depth, would be unstable in the same sense as it was initially since the unsaturated neutrally buoyant air within the thermal has a smaller θ_e than the surrounding dry air (unless the thermal "undershoots" the cloud base). Since the instability is always greatest for perturbations of small horizontal cross section, it would appear that at some point in its descent the thermal will break up into smaller entities. It proves useful to examine certain properties of dry thermals in this context.

Scorer (1957) examined the properties of the downward convection of discrete masses of fluid released within a homogeneous fluid of smaller density. His observations show that the motion resembles that of a spherical vortex (e.g., Lamb, 1945), with descent along the axis of symmetry and ascent along the periphery. The leading edge of the thermal is relatively smooth despite the static instability in this region, while the trailing edge is highly turbulent. The lack of strong turbulence along the leading edge is perhaps due to the fact that instabilities which do develop are swept around the leading edge before they can grow to substantial amplitude. In any event, the stability of the leading edge is associated with some aspect of the relative flow.

In dry thermals or plumes, the maximum magnitudes of the buoyancy and vertical velocity generally occur near the central axis, and the radial profiles are observed to conform roughly to Gaussian distributions. As the penetrative downdraft contains an unsaturated core and since most of the evaporation may occur away from the central axis, such a distribution may not be maintained and geometric similarity should break down at some point. The magnitude of the negative buoyancy should decrease and perhaps even reverse sign as the downdraft expands, leading to reversed momentum generation along the central axis and a breakup of the downdraft into smaller entities. This branching behavior should continue indefinitely, as long as there remains cloud water available for evaporation and as long as the equivalent potential temperature of the cloud decreases upward. The length of each branch will be proportional to $(M - g)N^{-2}l_c$, as expressed by (31). Thus an inert cloud whose top is unstable by the criterion developed by Randall (1980) will continue to cool and dry through its entire depth by the action of the penetrative thermals until the cloud top criterion can no longer be satisfied, or until the cloud dissipates entirely. It should also be pointed out that since the cloud top may be unstable to penetrative disturbances even when it is statically stable, the cloud may continue to dissipate even after the bulk of it is in hydrostatic equilibrium with its environment. Thus the "equilibrium cloud" proposed by Telford (1975) may still be unstable to penetrative disturbances, although a means of initiating those disturbances may be absent in that case.

TABLE 2. Maximum penetration depth and vertical velocity of penetrative thermals as a function of cloud liquid water content. Calculations are performed assuming the thermal remains unsaturated, and for $N^2 = 5 \times 10^{-5}$ s^{-2}, $\alpha = 0.285$, $M = 82$ m^2 s^{-1} and $F_0 = 10^5$ m^4 s^{-2}. The results are insensitive to both α and F_0 except when $l_c = 0$.

l_c (g kg^{-1})	$-z_{max}$ (km)	$-w_{max}$ (m s^{-1})
0	0.91	—
0.5	1.65	2.92
1	3.30	5.83
2	6.60	11.67
3	9.90	17.50
4	13.20	23.34
5	16.50	29.17

5. Cumulus clouds and penetrative downdrafts

The pervasive and strong instability of inert clouds to deeply penetrating downdrafts initiated at their tops carries strong implications for the development of cumulus clouds. Not only are the summits of developing cumulus clouds unstable in the classical sense but, in general, they are also unstable to the penetrative downdraft. While the previously discussed similarity theory for such thermals is clearly inadequate for the detailed treatment of penetrative convection in cumulus clouds, which are highly turbulent and whose tops are globally rather than locally unstable, the theory does suggest that penetrative convection will occur under a wide variety of circumstances and with characteristic velocities comparable to those associated with convective ascent. Indeed, it would appear that the only moist convective motions immune to the influence of penetrative downdrafts are those within clouds whose tops do not meet the cloud-top instability criterion and those associated with quasi-steady convective updrafts which are so intense as to preclude the penetration of downdrafts from aloft. The existence of regions of essentially moist-adiabatic ascent within severe thunderstorms (Heymsfield *et al.*, 1978) provides

supporting evidence for these possibilities and lends further credence to the notion that entrainment from the sides of the cloud is comparatively insignificant.

The idea, first suggested by Squires (1958), that penetrative downdrafts dominate the mixing process within cumuli has been strongly reiterated by Telford (1975), who stressed that direct observations of cumulus clouds strongly support this premise in preference to the lateral entrainment model. The relevant observations are:

1) The liquid water content of cumuli is well below its adiabatic value, and its ratio to the latter is generally a decreasing function of height (Warner, 1955; Squires, 1958). The importance of some mechanism of entrainment of environmental air is thus illustrated.

2) The liquid water in cumulus clouds shows no systematic tendency to peak near the center of the cloud, and large dry gaps are commonly observed (Warner, 1955). These observations contradict the premise of the lateral entrainment model.

3) The maximum water content of cumulus clouds is not a function of their width (Warner, 1955), as would be implied by lateral entrainment theory.

4) The strongest mixing occurs near the cloud top (Warner, 1977).

To these observations we can now add the results of Paluch (1979) who examined glider observations of large, nonprecipitating cumulus clouds in Colorado. As has been mentioned in the Introduction, Paluch's results demonstrate that the observed cloudy air within the cumuli she studied represents a mixture of subcloud-layer air and environmental air near the cloud top, with little influence from environmental air from near the cloud top.

The objections to the lateral entrainment model raised by the observations are supported by the fact that one-dimensional steady-state models built on the lateral entrainment assumption consistently predict excessive liquid water contents when the simulated cloud top is made to conform with the observations, as has been pointed out by Warner (1970), who suggested that such simulations are essentially exercises in empirical curve fitting. By contrast, a simple model proposed by Telford (1975) assumes that actual clouds are far closer to a state of hydrostatic equilibrium with their environment than they are to a state wherein the cloud properties reflect moist adiabatic ascent. Telford argues that the equilibrium is achieved by the mixing of environmental air at cloud top with cloudy air at each level within the cloud. The equilibrium clouds computed using several thermodynamic soundings have liquid water distributions which are closer to those of observed clouds than can be achieved with models which rely on lateral entrainment.

One problem which arises in applying the previous calculations to cumulus clouds is the assumption of constant liquid water content; this assumption implies that some sedimentation of cloud water has occurred. It is instructive to consider the case of a two-step process in which air from a well-mixed subcloud layer is moist adiabatically lifted to a prescribed level and then subject to the action of penetrative downdrafts. We permit no sedimentation of liquid water so that both the liquid water static energy h_l and the moist static energy h_m are nearly conservative.

At each level in the resulting cloud a fraction ϵ of cloudy air originating in the subcloud layer is mixed with a fraction $1 - \epsilon$ of air from the prescribed cloud-top environment in such a way that the resulting mixture is just saturated and contains no liquid water. This mixture will have the maximum possible temperature deficit compared to the surrounding cloud. Although this temperature deficit is not precisely equivalent to the buoyancy of the mixture, we can use its value to assess the potential for downdrafts at various levels in the cloud.

The saturation mixing ratio of the mixture may be estimated using (12) under the assumption that the temperature deficit is very small compared to the mean temperature. We obtain

$$q_{sm} \approx q_c[1 + a(s_m - s_c)], \tag{34}$$

where q_{sm} is the saturation mixing ratio of the mixture, q_c the mixing ratio of the cloud, s_m and s_c the dry static energies of the mixture and cloud respectively, and a a constant equal to $L_v/R_v c_p \bar{T}^2$. Since total water is conserved and the mixture contains no liquid water, its vapor mixing ratio is

$$q_m = \epsilon q_b + (1 - \epsilon) q_t, \tag{35}$$

where q_b and q_t are the vapor mixing ratios of the boundary-layer air and cloud-top environment, respectively. The value of ϵ which makes the mixture just saturated is obtained by equating (34) and (35):

$$\epsilon = \frac{q_{sm} - q_t}{q_b - q_t}. \tag{36}$$

Since s_m depends on ϵ in (34), the above relation is implicit for ϵ.

We now find the temperature deficit (dry static energy deficit) of the mixture using the value of ϵ given by (36). Since liquid water static energy h_l is conserved during the mixing, we have

$$h_{lm} = \epsilon h_{lb} + (1 - \epsilon) h_{lt},$$

where h_{lb} and h_{lt} are the values of h_l in the subcloud-layer and cloud-top environment, respectively. Since the mixture, the subcloud layer, and the cloud-top environment all contain no liquid water, h_l is in each case equivalent to the dry static energy s. Thus we have

$$s_m = \epsilon s_b + (1 - \epsilon) s_t, \tag{37}$$

where the subscripts have the usual meaning. At each level in the cloud, the dry static energy may, by virtue of conservation of h_l, be expressed as

$$s_c = s_b + L_v l_a, \tag{38}$$

where l_a is the adiabatic value of the cloud liquid water mixing ratio. Using (36) for ϵ in (37), and making use of the fact that $l_a = q_b - q_c$, we obtain, after some manipulation of (37) and (38),

$$s_c - s_m = l_a \frac{h_b - h_t}{q_b - q_t + aq_c(s_t - s_b)}, \tag{39}$$

where h_b and h_t are the moist static energies of the subcloud layer and cloud-top environment, respectively. After noting that $q_b - q_t$ and $s_t - s_b$ are typically positive, we see that whenever $h_b > h_t$ a mixture of air from above cloud top with air from the subcloud layer can always be found which is colder than the cloud air. Also, since l_a increases upward from zero at cloud base while q_c decreases upward, the maximum possible temperature deficit increases upward from zero at cloud base, according to (39). Even when the effects of liquid water and water vapor on density are considered, it is apparent from (39) or (37) that a negatively buoyant downdraft is impossible at cloud base unless some sedimentation of liquid water has occurred. In that case, h_l is not conserved and it is possible to generate negative buoyancy at cloud base. We shall later return to this point in discussing a possible mechanism for downbursts.

Finally, it may be noted that the dominant role of penetrative downdrafts in cumulus dynamics, implied by both observations and the present work, casts some doubt on the validity of many numerical simulations of small convective clouds performed to date. The very small horizontal scale together with the substantial vertical extent of penetrative downdrafts suggest that they can neither be resolved explicitly within most models, nor can their existence be accounted for through the use of the type of turbulence parameterizations currently employed. An important exception might be the simulation of large convective storms with stable ice anvils, above which θ_e is too high to permit the formation of penetrative downdrafts (see Section 5), or whose quasi-steady updrafts are so strong as to prevent the downdrafts from penetrating substantial depths into the clouds. Numerical simulations of this type of cloud have been relatively successful (e.g., Klemp and Wilhelmson, 1978). For smaller clouds, some progress has been made in representing penetrating downdrafts, most noteably by Raymond (1979) who treats moist convection as a two-scale process that accounts for the penetrative downdrafts. His model is successful in producing realistic distributions of liquid water, velocity and turbulence, especially when these quantities are compared to those produced by lateral entrainment models. These results, together with the evidence presented here, suggest that the failure to account for the presence of penetrative downdrafts in most cumulus clouds may lead to a serious misrepresentation of their dynamics.

6. Mamma formations and cloud-based detrainment instability

An unusual form of downward convection is sometimes observed on the underside of middle- or high-based stratiform clouds, most frequently those associated with outflow from strong thunderstorms. The convection takes the form of downward projecting protuberances often of highly laminar appearance, on the underside of the clouds, which are sometimes high enough to be composed mostly of ice crystals. A photograph of one such formation is presented in Fig. 2. Although the individual elements are highly laminar in appearance, aircraft flying through their cores encounter moderate to strong turbulence (Hlad, 1944). Ludlam and Scorer (1953) attribute mamma to conditional instability resulting from the simultaneous moist adiabatic and dry adiabatic descent of the cloud air and subcloud air, respectively, but decline to offer an explanation of the laminar appearance of the clouds.

A possible alternative explanation for mamma is that they are manifestations of undershooting penetrative thermals initiated at the cloud tops. The results of the previous section indicate, however, that the saturation vapor pressure and its vertical lapse rate are too small at the altitudes at which mamma are commonly observed to permit the rapid growth of penetrative downdrafts. It is not clear that the cloud top instability criterion is ever satisfied at the tops of cirrus anvils which frequently penetrate into the lower stratosphere, nor is it certain that the ice crystals within the anvil can evaporate rapidly enough to drive substantial downdrafts.

A more attractive alternative is that mammatus formations result from another cloud instability which was first discussed by Scorer (1972). The instability is analogous to cloud-top entrainment instability and, as it occurs at the cloud base, might be called Cloud-Base Detrainment Instability (CBDI). This occurs when cloudy air overlies unsaturated air with a higher value of liquid water static energy. The mechanism of CBDI is illustrated in Fig. 3. If cloudy air is mixed downward into unsaturated air with a larger value of h_l and just enough mixing occurs to evaporate all of the liquid water in the cloudy air, the resulting mixture will be negatively buoyant with respect to the surrounding air. This is so because in the absence of precipitation h_l is both moist-adiabatically conservative and linearly mix-

FIG. 2. A display of mammatus on the underside of a cumulonimbus anvil. (Photo courtesy of David Hoadley.)

able, so that the resulting mixture will have an h_l lower than the surrounding air. Since in the absence of liquid water $h_l = s$, the mixture is negatively buoyant and will accelerate downward. The instability criterion is then

$$\Delta h_l < 0 \tag{40}$$

and $q < q^*$ below cloud base, where Δh_l is the jump in liquid water static energy across cloud base, and q and q^* are the mixing ratio and saturation mixing ratio, respectively, of subcloud-base air. The above criterion neglects the effect of water vapor on density.

Since, in general, the air ascending into a cloud base will approach saturation and since the cloud water increases upward from zero at cloud base, CBDI must be limited to clouds resulting from the horizontal advection of cloudy air over clear air, as in the case of a thunderstorm anvil. The instability is a consequence of the differential advection of h_l.

The dynamics of individual CBDI thermals are in some ways similar to those of penetrative downdrafts. CBDI also relies on mixing and should therefore seek small scales. Unlike the penetrative downdrafts, however, CBDI thermals rapidly exhaust their initial liquid water supply and quickly lose their negative buoyancy as a result. Such thermals can not therefore be expected to penetrate very far into the subcloud environment.

A similarity solution for CBDI thermals is here pursued under the same justification as was provided for the solutions for penetrative downdrafts. We assume here that the liquid water within the thermal is evaporated at a rate just sufficient to keep the thermal saturated. Other assumptions used are as in the case of penetrative thermals. The conservation equations for the spherical CBDI thermal are

$$\frac{d}{dz}R^3 = -3\alpha R^2 \qquad \text{mass,} \tag{41}$$

$$\frac{d}{dz}R^6w^2 = 2R^6(B - gl) \quad \text{momentum,} \tag{42}$$

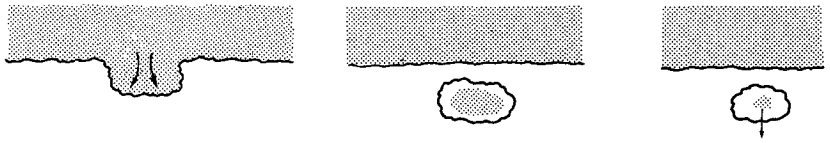

a) A cloudy parcel is detrained into dry, sub-cloud air

b) Mixing with the sub-cloud air causes evaporation

c) The negatively buoyant parcel accelerates downward

FIG. 3. Illustration of the mechanism of cloud-base detrainment instability.

$$\frac{d}{dz}R^3(B - Ml) = -R^3N^2 \qquad \text{heat,} \tag{43}$$

$$\frac{d}{dz}R^3(q_s + l - q_e) = -R^3\frac{dq_e}{dz} \qquad \text{water surplus,} \tag{44}$$

where l is the thermal's liquid water content, q_s the (saturation) mixing ratio within the thermal, and q_e the environmental mixing ratio. We define volume-integrated heat and water surpluses as

$$F = R^3B$$

and

$$Q = R^3(q_s + l - q_e).$$

The initial conditions for the set (41)–(44) are then

$$\left.\begin{aligned} R = w &= 0 \\ F &= F_0 \\ Q &= Q_0 \end{aligned}\right\} \quad \text{at} \quad z = 0. \tag{45}$$

For simplicity, we examine the case where the sub-cloud mixing ratio is constant. Then by (44) $Q = Q_0$ for all z and the solutions for the thermal's radius and liquid water content are

$$R = -\alpha z, \tag{46}$$

$$l = -\frac{Q_0}{\alpha^3 z^3} + q_e - q_{es}\exp\left(\frac{L_v}{R_v\bar{T}g}B\right), \tag{47}$$

where q_{es} is the environmental saturation mixing ratio and the Clausius-Clapeyron equation has been used to relate the saturation mixing ratio of the thermal to that of the environment. The solution of the heat equation (43) follows under the assumption that N^2 is constant and that l is nonzero. Because of the dependence of l on B in (47), the solution must be written in implicit form:

$$B + Mq_{es}\exp\left(\frac{L_v}{R_v\bar{T}g}B\right) = \frac{-F_0}{\alpha^3 z^3} + Mq_e - \frac{1}{4}N^2 z. \tag{48}$$

Due to the form of (48), an exact analytic solution to the momentum equation (42) is not available. One may nevertheless estimate the maximum penetration depth of the thermal by finding the levels at which the liquid water and temperature deficit of the thermal vanish, using (47) and (48), respectively. If the temperature deficit is small enough that the last term in (47) can be assumed equal to q_{es}, then

$$l = 0 \quad \text{at} \quad -z \approx \alpha^{-1}(q_{es} - q_e)^{-1/3}Q_0^{1/3}. \tag{49}$$

The level of vanishing temperature deficit is estimated by assuming that the first term on the right of (48) is negligible at this level. This will be true if

$$(q_{es} - q_e) \gg 2^{-3/2}(-F_0)^{1/4}\alpha^{-3/4}N^{3/2}M^{-1}.$$

Then

$$B = 0 \quad \text{at} \quad -z \approx 4MN^{-2}(q_{es} - q_e). \tag{50}$$

The penetration depth of the thermal will be slightly greater than the values given in (49) or (50), whichever is smaller. Note that the instability is most prominent in environments of moderate relative humidity; if the environment is too dry the thermal loses its liquid water content very rapidly, while when the environment is moist the evaporation proceeds too slowly to sustain the negative buoyancy against adiabatic warming. In the latter case branching behavior is perhaps a possibility.

An order-of-magnitude estimate of vertical velocities characteristic of CBDI thermals can be made using (42). Assuming, for this purpose, that the exponential terms in (47) and (48) are order unity, (42) integrates to

$$w^2 \approx \tfrac{1}{2}(gQ_0 - F_0)\alpha^{-3}z^{-2} - \tfrac{2}{7}(m - g) \times (q_{es} - q_e)z - \tfrac{1}{16}N^2z^2. \tag{51}$$

Assuming that the thermal retains its liquid water until the maximum velocity has been attained, the maximum velocity predicted by (41), ignoring the first term on the right, is

$$-w_{\max} \simeq \tfrac{4}{7}(m - g)N^{-1}(q_{es} - q_e). \tag{52}$$

For values of these parameters likely to be encountered in the environment of mamma, this maximum vertical velocity is on the order of a few meters per second. Warner (1973) reports vertical velocities of mamma elements of between -1.2 and -3.1 m s^{-1}, with a mean of -2.3 m s^{-1}.

It is necessary also to explain the very laminar appearance of mamma (Fig. 2) and to account for

TABLE 3. Evaporation rates of cumulonimbus ice crystals exposed to an environment of 70% relative humidity, p = 400 mb and T = 240 K. I_i is the ice water content of crystals of average length L_i. τ_i is an evaporation time scale = $0.57L_i/(dL_i/dt)$.

L_i (mm)	I_i [10^{-3} g m^{-3} (size cat.)$^{-1}$]	$-\frac{dI_i}{dt}$ [10^{-6} g m^{-3} (size cat.)$^{-1}$ s^{-1}]	τ_i (s)
0.07	1.32	9.23	143
0.21	7.79	17.68	523
0.36	13.74	19.56	924
0.50	23.22	23.69	1294
0.64	26.78	27.37	1665
0.79	30.39	23.35	2035
0.93	36.29	18.34	2405
1.08	47.39	22.15	2804
1.25	51.09	25.49	3236
1.42	57.49	19.71	3668
1.58	69.72	17.01	4098
1.75	83.01	27.04	4530
1.92	81.92	16.51	4963
⋮	⋮	⋮	⋮

Approximate summed quantities:

$I = 0.53$ g m^{-3}

$\frac{dI}{dt} = 2.67 \times 10^{-4}$ g m^{-3} s^{-1}

$\tau\left[=I\left(\frac{dI}{dt}\right)^{-1}\right] = 1984$ s = 33 min.

their presence in ice clouds. Until recently, there has been very little in the way of either observations of ice spectra within clouds or theoretical estimates of evaporation rates of ice crystals in sub-saturated air. Hall and Pruppacher (1976) have shown that the time rate of change of ice crystal length due to sublimation is independent of crystal length for crystals of length > 0.2–0.3 mm. For crystals of smaller length, the rate of change of length increases with decreasing length. Heymsfield and Knollenberg (1972) have shown that the ice-water content of cirrus clouds comprised of bullet crystals may be expressed as

$$I\ [\text{g m}^{-3}] = 1.65 \times 10^{-5} \sum_{i=1}^{N} N_i L_i^{1.74}, \qquad (53)$$

where N_i is the number of particles per cubic meter of length L_i [mm]. Under the assumption that the total number of size categories N is not a function of time, the above may be differentiated in time with the result that

$$\frac{dI}{dt}\ [\text{g m}^{-3}\ \text{s}^{-1}] = \sum_{i=1}^{N} A_i \frac{dL_i}{dt}\ , \qquad (54)$$

where

$$A_i \equiv -\left[\frac{I_{i+1}L_{i+1}^{-1.74} - I_{i-1}L_{i-1}^{-1.74}}{L_{i+1} - L_{i-1}}\right] L_i^{1.74} + 1.74\,\frac{I_i}{L_i}\ . \qquad (55)$$

and I_i is the ice water content within the size category i. The second term on the right of (55) represents the contribution to the evaporation rate from the evaporation within each size category, while the first term is a finite-difference approximation for the rate at which ice crystals enter category i. Since dL_i/dt is approximately constant, one can see by inspection of (54) and (55) that evaporation rates will be larger if much of the ice water is contained in small crystals.

Measurements of size spectra within cirrus clouds have been presented by Heymsfield and Knollenberg (1972). These measurements show that while the number concentration of ice crystals has a distinct peak at ~0.5 mm in most cirrus clouds, the spectrum peaks at the smallest size category measured within cirrus anvils associated with cumulonimbus clouds. This suggests that evaporation of ice may proceed rapidly enough in cirrus anvils to drive CBDI thermals. Table 3 shows calculations of the evaporation rates within each size category measured within a cumulonimbus anvil, using the measurements of Heymsfield and Knollenberg (1972) and the evaporation model presented by Hall and Pruppacher (1976), assuming a pressure of 400 mb, a temperature of 240 K and a relative humidity of 70%. Table 4 lists similar calculations for cirrus uncinus clouds. (Here, the positive rate of change of ice water content in the smaller categories results from the additions to those categories from the shortening of crystals in larger categories.)

If the similarity theory for either penetrative downdrafts or CBDI thermals is to be applied to an ice cloud one must have evaporation time scales similar to the advective time scale of the similarity thermal. The latter time scale is approximately

TABLE 4. Evaporation rates of cirrus uncinus ice crystals exposed to an environment of 70% relative humidity, p = 400 mb and T = 240 K. I_i is the ice water content of crystals of average length L_i. τ_i is an evaporation time scale [$\tau_i = 0.57L_i/(dL_i/dt)$].

L_i (mm)	I_i [10^{-3} g m^{-3} (size cat.)$^{-1}$]	$-\frac{dI_i}{dt}$ [10^{-6} g m^{-3} (size cat.)$^{-1}$ s^{-1}]	τ_i (s)
0.167	0.22	−0.62	288
0.333	0.49	−2.96	638
0.500	9.88	−1.69	958
0.667	23.65	9.69	1278
0.833	38.42	34.89	1596
1.000	31.35	56.46	1916
1.167	10.79	39.81	2236
1.333	2.72	9.63	2554
1.500	5.01	4.74	2874

Approximate summed quantities:

$I = 0.122$ g m^{-3}

$\frac{dI}{dt} = 1.50 \times 10^{-4}$ g m^{-3} s^{-1}

$\tau = 813$ s.

$$\tau_{\text{thermal}} \sim \left(\frac{w}{l}\frac{dl}{dz}\right)^{-1}.$$

Estimating l and w from (47) and (52), respectively, we have

$$\tau_{\text{thermal}} \sim (m - g)^{-1}N(q_{es} - q_e)^{-1}z$$

for the CBDI thermal. Using (49) as an estimate for z there results

$$\tau_{\text{thermal}} \sim (m - g)^{-1}N(q_{es} - q_e)^{-4/3}\alpha^{-1}Q_0^{1/3}. \quad (56)$$

For typical values of the parameters which appear in (56), this amounts to a time scale of roughly 50–500 s. Comparing these values to those associated with the evaporation of ice (Tables 3 and 4), it is seen that the downward propagation of thermals in ice clouds will be considerably damped by the effect of the long time scale associated with the evaporation of ice. It is likely that large ice crystals will remain within the mamma elements even after they have passed their level of neutral buoyancy, accounting for their opaque appearance. The laminar character of the visible elements may be attributable to the strong static stability at their leading edges after they have "undershot" their equilibrium level, although it must be admitted that the elements even appear laminar early in their development.

Another possibility, suggested by a reviewer, is that the broad spectrum of particle sizes and associated fallspeeds within mamma elements smooths out their visible boundaries even in the presence of some small-scale turbulence. This would not occur in upward-expanding buoyant elements which contain only small particles.

Finally, the effect of CBDI convection on the immediate subcloud environment will be to cool the air just below cloud base, establishing a dry-adiabatic lapse rate in this region and an inversion at cloud base. Neutral stability to CBDI perturbations will occur when the jump of dry static energy across cloud base is

$$\Delta s = L_v \Delta l.$$

Measurements of the thermodynamic structure of the near-cloud-base environment of outflow clouds would thus provide evidence for the occurrence of CBDI convection.

7. Downbursts

The term "downburst" has been introduced by Fujita (Fujita and Byers, 1977) to describe exceptionally strong, very small-scale downdrafts within intense thunderstorms. These downdrafts have typical horizontal dimensions of 500–2000 m and are thus almost an order-or-magnitude smaller than the general region of descending air within large thunderstorms. The downbursts are sometimes powerful enough to cause damage at the surface; the damage patterns attest to the very small scale of the downdrafts (e.g., Fujita and Byers, 1977). Downbursts present a major hazard to aircraft (Fujita and Byers, 1977; Fujita and Caracena, 1977).

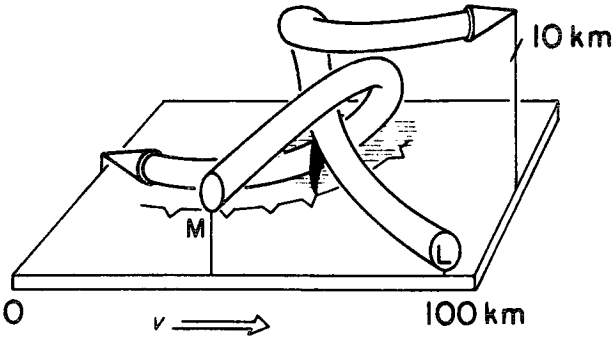

FIG. 4. Schematic air flow in and around a right-moving supercell thunderstorm. M and L denote middle- and low-level air, respectively. The region of precipitation is shown by hatching, and the approximate locations of the gust front and tornado (when present) are shown. (After Browning, 1964.)

The general subsiding motion in the downdraft region of thunderstorms is thought to be a consequence of the evaporation (and melting) of precipitation falling into dry air entering from the middle troposphere (e.g., Ludlam, 1963). The scale of such a draft is determined by the scale of the region of falling precipitation and is thus of the same order as the dimensions of the main updraft. The side-by-side arrangement of updraft and downdraft is evident in strong thunderstorms in environments of considerable low- and middle-level ambient wind shear; together they constitute the dynamical system which is the storm itself. The comparatively small scale of downbursts suggests that these are a consequence of a dynamically distinct mechanism. We here propose that penetrative downdrafts are responsible for downbursts and account for their high intensity and small scale.

The potential for intense penetrative downdrafts within severe convective storms appears as a consequence of the associated strong negative vertical gradient of equivalent potential temperature in the lower troposphere together with the nearly adiabatic liquid water content of the main updraft. Observations (e.g., Marwitz, 1972) and numerical simulations (e.g., Klemp and Wilhelmson, 1978) reveal strong systematic entrainment of potentially cold environmental air at middle levels in the storm, particularly along the forward edge of the storm. In the right-moving supercell storm (Fig. 4) the middle-level potentially cold air appears to enter the storm from the right-front quadrant, traveling over and cyclonically around the main updraft (Browning, 1964; Klemp and Wilhelmson, 1978). The superposition of the dry potentially cold air over cloudy air which

has very high liquid water content suggests a strong potential for intense penetrative downdrafts. The potential for strong evaporative cooling is enhanced by the small median diameter of the water drops which characterize the radar vault region of the updraft. The instability may be realized when the cloud air of high liquid water content loses its upward velocity due to liquid water loading or dynamically induced downward pressure gradients, allowing the potentially cold air to penetrate downward from middle levels. It should be noted that the ability of potentially cold air to penetrate to the surface with a substantial temperature deficit depends on the existence of precipitation at least somewhere along the trajectory of the downdraft, as demonstrated in Section 5.

One specific possible scenario for the occurrence of a downburst involves the mesocyclone of supercell storms. In one such mesocyclone studied by Brandes (1978), the rotation of the lower region of the mesocyclone was apparently sufficient to stop the updraft through the "vortex valve" effect, leaving a column of air with high liquid water content and small vertical velocity near the mesocyclone center directly below a region of inflowing potentially cold air (see Brandes, 1978, Fig. 7). Doppler measurements of the storm do show a small region of strongly descending air near the mesocyclone center, though this may be due to the adverse vertical pressure gradient associated with the aforementioned vortex valve effect, as discussed by Brandes (1978). A close association between downbursts and mesocyclones has been noted recently by Forbes and Wakimoto (1981).

It would appear that the very small scale of downbursts precludes the possibility that they have been simulated by current numerical thunderstorm models (e.g., Schlesinger, 1978; Klemp and Wilhelmson, 1978; Clark, 1979), though these models should be capable of explicitly resolving penetrative downdrafts if the model resolution is greatly increased. The possible significance of penetrative downdrafts in overall thunderstorm evolution, as well as the potential hazard they may pose under extreme circumstances warrants further investigation of their dynamical characteristics.

8. Conclusions

A similarity theory describing the properties of unsaturated penetrative downdrafts initiated at the top of deep, inert clouds has been presented; it is argued that the use of such theory is justified by the very small scale of individual penetrative elements. An equivalent theory has been applied to the description of thermals resulting from Cloud-Base Detrainment Instability (CBDI). The results show that provided the cloud-top instability criterion is met, unsaturated downdrafts may penetrate deep into clouds, with velocities comparable to those associated with the buoyant updrafts. The theory also suggests that individual thermals or plumes may branch into a number of similar entities after having penetrated a certain distance into the cloud. Under special conditions sometimes associated with severe convective storms, penetrative downdrafts may be sufficiently intense to cause damage at the surface and are perhaps related to downbursts, as described by Fujita and Byers (1977). In the latter case, the drafts, rather than being initiated at the top of the cloud, may instead result from the systematic entrainment of potentially cold air at middle levels within the storm cloud.

CBDI thermals may account for mamma formations in water clouds or those ice clouds in which much of the cloud ice is contained in very small crystals.

Finally, we emphasize that the results of the present analysis, taken together with the myriad observations of small and moderate cumulus clouds, strongly suggest that classical entrainment models developed on the basis of laboratory experiments do not apply when phase changes of water substance are important to the thermodynamics and must finally be abandoned in favor of models in which mixing through the cloud top dominates the internal dynamics of the clouds. The small horizontal scale of the individual penetrative elements, coupled with the large vertical distances which they traverse, would appear to render useless most of the turbulence parameterizations currently used in cumulus models, except perhaps for those models with exceptional resolution or which describe clouds whose tops are too high or whose quasi-steady updrafts are too strong to permit the penetration of potentially cold air from above. A radically new approach to cumulus modelling, such as that proposed by Raymond (1979), seems necessary. The recognition of the importance of cloud-top instability in cumulus dynamics ought to lead to a reassessment of the understanding of the interaction of cumulus clouds with the large-scale environment, and so should influence future efforts to parameterize this interaction.

Acknowledgments. Part of the research leading to the present results was performed while the author was visiting the National Center for Atmospheric Research.[2] May I express my sincere gratitude to William Hall of NCAR, who performed several microphysical calculations for the author, to Edwin Kessler of the National Severe Storms Laboratory for his enlightening discussions on the subject of downbursts, and to David Raymond of New Mexico Institute of Mining and Technology who pointed out

[2] The National Center for Atmospheric Research is sponsored by the National Science Foundation.

the role of precipitation in downdrafts which reach the surface. The author also is grateful for numerous constructive suggestions made by one of the reviewers.

REFERENCES

Batchelor, G. K., 1954: Heat convection and buoyancy effects in fluids. *Quart. J. Roy. Meteor. Soc.*, **80**, 339–358.

Brandes, E. A., 1978: Mesocyclone evolution and tornadogenesis: Some observations. *Mon. Wea. Rev.*, **106**, 995–1011.

Browning, K. A., 1964: Airflow and precipitation trajectories within severe local storms which travel to the right of the winds. *J. Atmos. Sci.*, **21**, 634–639.

Clark, T. L., 1979: Numerical simulations with a three-dimensional cloud model: Lateral boundary condition experiments and multicellular severe storm simulations. *J. Atmos. Sci.*, **36**, 2191–2215.

Deardorff, J. W., 1980: Cloud top entrainment instability. *J. Atmos. Sci.*, **37**, 131–147.

Forbes, G. S., and R. M. Wakimoto, 1981: Tornadoes associated with gust fronts and downbursts. *Mon. Wea. Rev.*, **109** (in press).

Fujita, T. T., and H. R. Byers, 1977: Spearhead echo and downbursts in the crash of an airliner. *Mon. Wea. Rev.*, **105**, 129–146.

——, and G. Caracena, 1977: An analysis of three weather-related aircraft accidents. *Bull. Amer. Meteor. Soc.*, **58**, 1164–1181.

Hall, W. D., and H. R. Pruppacher, 1976: The survival of ice particles falling from cirrus clouds in subsaturated air. *J. Atmos. Sci.*, **33**, 1995–2006.

Heymsfield, A. J., and R. G. Knollenberg, 1972: Properties of cirrus generating cells. *J. Atmos. Sci.*, **29**, 1358–1366.

——, P. N. Johnson and J. E. Dye, 1978: Observations of moist adiabatic ascent in northeast Colorado cumulus congestus clouds. *J. Atmos. Sci.*, **35**, 1689–1703.

Hlad, C. J., 1944: Stability-tendency and mammatocumulus clouds. *Bull. Amer. Meteor. Soc.*, **25**, 327–331.

Klemp, J. B., and R. B. Wilhelmson, 1978: Similations of right- and left-moving storms through storm splitting. *J. Atmos. Sci.*, **35**, 1097–1110.

Lamb, H., 1945: *Hydrodynamics*. Dover, 738 pp.

Ludlum, F. H., 1963: Severe local storms: A review. *Severe Local Storms, Meteor. Monogr.*, No. 27, Amer. Meteor. Soc. 247 pp.

——, and R. S. Scorer, 1953: Convection in the atmosphere. *Quart. J. Roy. Meteor. Soc.*, **79**, 317–341.

Malkus, J. S., 1954: Some results of a trade cumulus cloud investigation. *J. Meteor.*, **11**, 220–237.

Marwitz, J. D., 1972: The structure and motion of severe hailstorms. Part I: Supercell storms. *J. Appl. Meteor.*, **11**, 166–179.

McCarthy, J., 1974: Field verification of the relationship between entrainment rate and cumulus cloud diameter. *J. Atmos. Sci.*, **31**, 1028–1039.

Morton, B. R., G. Taylor and J. S. Turner, 1956: Turbulent gravitational convection from maintained and instantaneous sources. *Proc. Roy. Soc. London*, **A234**, 1–23.

Paluch, I. R., 1979: The entrainment mechanism in Colorado cumuli. *J. Atmos. Sci.*, **36**, 2462–2478.

Randall, D. A., 1980: Conditional instability of the first kind upside-down. *J. Atmos. Sci.*, **37**, 125–130.

Raymond, D. J., 1979: A two-scale model of moist, non-precipitating convection. *J. Atmos. Sci.*, **36**, 816–831.

Schlesinger, R. E., 1978: A three-dimensional numerical model of an isolated thunderstorm: Part I. Comparative experiments for variable ambient wind shear. *J. Atmos. Sci.*, **35**, 690–713.

Schmidt, W., 1941: Turbulent propagation of a stream of heated air. *Z. Angew. Math. Mech.*, **21**, 265 and 351.

Scorer, R. S., 1957: Experiments on convection of isolated masses of buoyant fluid. *J. Fluid Mech.*, **2**, 583–594.

——, 1972: *Clouds of the World*. Stackpole Books, 176 pp.

Squires, P., 1958: Penetrative downdraughts in cumuli. *Tellus*, **10**, 381–389.

Stommel, H., 1947: Entrainment of air into a cumulus cloud. *J. Meteor.*, **4**, 91–94.

Telford, J. W., 1975: Turbulence, entrainment and mixing in cloud dynamics. *Pure Appl. Geophys.*, **113**, 1067–1084.

Warner, C., 1973: Measurements of mamma. *Weather*, **28**, 394–397.

Warner, J., 1955: The water content of cumuliform cloud. *Tellus*, **7**, 449–457.

——, 1970: On steady-state one-dimensional models of cumulus convection. *J. Atmos. Sci.*, **27**, 1035–1040.

——, 1977: Time variation of updraft and water content in small cumulus clouds. *J. Atmos. Sci.*, **34**, 1306–1312.

——, and P. Squires, 1958: Liquid water content and the adiabatic model of cumulus development. *Tellus*, **10**, 390–394.